



The Enhancement of the Energetic Particle Intensities in ICMEs

Mengjiao Xu¹, Chenglong Shen^{1,2}, Yutian Chi¹, Yuming Wang^{1,2,3} , Qiang Hu⁴ , Gang Li⁴ , Zhihui Zhong¹, and Jiayi Liu¹
¹ CAS Key Laboratory of Geospace Environment, Department of Geophysics and Planetary Sciences, University of Science & Technology of China, Hefei, Anhui 230026, People's Republic of China; clshen@ustc.edu.cn

² CAS Center for Excellence in Comparative Planetology, University of Science and Technology of China, Hefei, People's Republic of China

³ Mengcheng National Geophysical Observatory, School of Earth and Space Sciences, University of Science and Technology of China, Hefei, 230026, People's Republic of China

⁴ Department of Space Science and CSPAR, The University of Alabama in Huntsville, Huntsville, AL 35805, USA

Received 2019 April 14; revised 2019 September 14; accepted 2019 September 16; published 2019 October 30

Abstract

The behavior of energetic particles in interplanetary coronal mass ejections (ICMEs) is of great interest. In general, due to the relatively closed magnetic structures of ICMEs, the energetic-particle intensities are usually depressed in them. However, previous studies have found some counterexamples. In this work, using protons with energies from ~ 200 keV to ~ 7 MeV observed by *Wind*/3dp as a measure, we check the proton intensity signatures of the 487 ICMEs between 1995 and 2017. A total of 12 ICMEs with extraordinary energetic-particle enhancements have been found, 9 of which are shock-interplanetary coronal mass ejection complex structures (S-ICMEs) and 3 that are isolated interplanetary coronal mass ejections (I-ICMEs). Comparing the two kinds of ICMEs, we find that energetic-particle intensities increase more in the S-ICMEs than in the I-ICMEs in all energy channels, especially in the high-energy channels. In addition, shocks inside energetic-particle-enhanced S-ICMEs are relatively fast and strong. These results indicate that shock-ICME interaction may be an effective local acceleration mechanism.

Key words: acceleration of particles – shock waves – Sun: heliosphere

1. Introduction

Interplanetary coronal mass ejection (ICME), which is characterized by distinct large-scale magnetic-field topology such as the enhanced magnetic-field strength and the long and smooth rotated magnetic-field vector (e.g., Burlaga et al. 1981), is considered to be an important factor that could significantly influence the energetic-particle intensities. Many previous studies have shown that the energetic-particle intensities are usually depressed in ICMEs, particularly in those traveling in the ecliptic plane (e.g., Lario et al. 2005; Malandraki et al. 2005; Cane & Lario 2006). Richardson (1997) found that near the ecliptic, entry into and exit from an ICME is typically accompanied by a decrease and a recovery, respectively, in the particle density over a range of rigidities. For protons with energies lower than 100 MeV, the intensity drop can be greater than 70%. They suggested that ejecta are predominantly closed magnetic structures, thus avoiding the easy access and exit of particles. Cane & Lario (2006) reported the energetic-particle response to the passage of a fast ICME observed by the *Advanced Composition Explorer* (ACE) spacecraft in 1998 September. This fast ICME drove a strong interplanetary shock that locally accelerated ions to more than 60 MeV at its arrival at 1 au. In this event, they found a sharp decrease of the low-energy ion intensities precisely in the ICME interval, which demonstrated that the penetration of shock accelerated particles into the ICME was restricted. In addition, Kallenrode (2001) studied the influence of the magnetic cloud on the propagation of the energetic particles with a numerical model. The simulation results showed that a magnetic cloud may act as a barrier for external energetic particles' propagation.

On the other hand, Shen et al. (2008; hereafter, Shen2008) pointed out that in shock-interplanetary coronal mass ejection

complex structures (S-ICMEs), which are formed by fast forward shocks overtaking preceding ICMEs, the behavior of energetic particles may be much different. They analyzed the behavior of energetic particles in a shock-magnetic cloud (MC) interacting complex structure observed by the ACE spacecraft on 2001 November 5, finding an extraordinary energetic-particle enhancements over the entire period of the shock-MC structure. This enhancement might be due to the combined effects of the shock and the MC boundaries: the shock can accelerate particles within the MC and the MC boundaries prevent the leakage of these accelerated particles. In addition to this event, energetic-particle enhancements also occurred in the S-ICME on 2017 September 7 (Shen et al. 2018). Therefore, not all ICMEs have reduced fluxes of energetic particles. At least in some S-ICMEs, energetic-particle intensities may be enhanced. However, do all S-ICMEs have enhanced energetic-particle intensities? This question still needs to be answered.

In this work, we develop a method to automatically determine whether the energetic-particle intensities increase in the ICMEs. Using *Wind*/3dp (Lin et al. 1995) proton flux data as a measure, a total of 12 ICMEs are found to have enhanced energetic-particle intensities. Among them, 9 are S-ICMEs. In Section 2, we introduce in detail the selection criteria of these events. A typical case of an ICME with increased energetic-particle intensities is shown. Section 3 introduces the 12 cases in detail. Based on whether there are shocks within the ICMEs, we further classify these 12 events into two groups. Comparisons of these two kinds of events are discussed in Section 4. Section 5 describes the properties of these 9 shocks in ICMEs. In Section 6, we will briefly discuss the possible acceleration mechanisms in the 3 ICMEs without shocks. Conclusions are presented in the last section.

2. Identification of ICMEs with Enhanced Energetic Particle Intensities

Considering that in most cases, the energetic-particle enhancements in ICMEs are small, we develop a method to automatically select energetic-particle-enhanced ICMEs to avoid the errors caused by naked-eye recognition. First, we search all the ICMEs observed by *Wind* from 1995 to 2017. The ICMEs during 1995–2015 are from Chi et al. (2016). In their work, the ICME identification criteria were (i) enhanced magnetic-field intensity, (ii) smoothly changing magnetic-field direction, (iii) declining profile of the solar-wind velocity, (iv) low proton temperature, (v) low proton plasma β , and (vi) bidirectional streaming of electrons. A structure is recognized as an ICME when it fits at least three of the criteria listed above. The online catalog can be found at http://space.ustc.edu.cn/dreams/wind_icmes/. In addition, we extend this catalog to the end of 2017 using the same criteria. In total, there are 487 ICMEs observed by *Wind* from 1995 to 2017.

To examine the variations of energetic-particle intensities near the ICMEs, we employ data from *Wind*/3dp, which measures omnidirectional fluxes of protons with energy from ~ 70 keV to ~ 7 MeV in nine channels (Lin et al. 1995). Here, we consider only seven higher-energy channels, which start from ~ 200 keV (~ 200 , ~ 330 , ~ 550 keV, ~ 1 , ~ 2 , ~ 4.5 , ~ 7 MeV).

Our goal is to find the ICMEs during which the energetic-particle intensities are enhanced, so we need to compare the energetic-proton intensities measured in the ICME intervals with those observed in the upstream and downstream. Here, we take 1–4 hr before and after the ICME interval as the upstream and downstream. We define the upstream and downstream intervals in this way based on two considerations: on one hand, the durations of upstream and downstream should not be too long because of the risk of including energetic particles accelerated by other structures. For example, if our upstream interval includes the shock driven by the ICME and the shock is accompanied by a shock spike, which is a peak in the intensity of energetic particles at the passage of an interplanetary shock caused by shock local acceleration, then the upstream energetic-particle intensities cannot represent background energetic-particle level. On the other hand, considering the diffusion of energetic particles in ICMEs and the possible little errors in the locations of ICME boundaries, the upstream and downstream intervals should not be too close to the ICME edge. Therefore, we think that 1–4 hr is a suitable time interval to define the upstream and downstream. For all 487 ICMEs, we calculate the median proton intensities in the upstream, ICME interval, and downstream ($\text{flux}_{\text{upstream}}$, $\text{flux}_{\text{ICME}}$, and $\text{flux}_{\text{downstream}}$, respectively) at each energy channel.

If in more than four channels, the proton intensities in the ICME are at least twice as large as those in the upstream ($\text{flux}_{\text{ICME}}/\text{flux}_{\text{upstream}} \geq 2$) and not lower than those in the downstream ($\text{flux}_{\text{ICME}}/\text{flux}_{\text{downstream}} \geq 1$), then this ICME is chosen as an energetic-particle-enhanced ICME. Using this automated selection method, we found 15 events. These 15 ICMEs are further cross-checked in terms of a coincidence with a solar eruption: if, by chance, the energetic particles accelerated by eruptions near the solar surface arrive at the spacecraft at the same time as an ICME passes, they would be wrongly counted as locally accelerated particles (e.g., Malandraki et al. 2002; Lario 2006; Saiz et al. 2008; Kahler et al. 2011; Tan et al. 2012). Therefore, the X-ray and solar-image

observations have been analyzed to exclude cases caused by solar activities. Meanwhile, if the locally observed protons in an ICME event show the velocity dispersion, which suggest that the particles are coming from far away, then the event will be excluded too. Because we just want to investigate the ICMEs in which energetic particles are enhanced during the whole intervals, we are not worried that our selection criteria might discriminate against cases in which a large energetic-particle enhancement of short duration lies inside a very long ICME. Just in case, we check the time lengths of the 487 ICMEs in our ICME catalog, finding that the durations vary from 2.5 to 93.6 hr with an averaged value of 21 hr. And if we focus on the 47 long ICMEs with durations greater than 40 hr, we can find that none of them have short durations of energetic-particle enhancements.

As an example, Figure 1 gives an overview of the energetic-particle-enhanced ICME event observed by the *Wind* spacecraft in 2003 May. The ICME is marked by the gray shaded region in the figure, with the signatures of enhanced magnetic-field strength and bidirectional suprathermal electron streaming. In the middle of this ICME, at 18:31UT on May 29, we can clearly find a fast forward shock (vertical dashed black line) based on the jump of the magnetic-field strength, velocity, and density. It means that this ICME is an S-ICME. The top panel of the figure shows the color-coded proton intensities. The ordinate is proton energy and the changes in color represent the changes in proton intensities. The second panel is the distribution of the proton enhancements relative to the median values in the upstream ($\text{flux}_{\text{upstream}}$) in different energy channels. Seen from this figure, the intensities of protons in all energy channels increase significantly at the ICME's front edge and decrease just after its trailing edge. In addition to the enhancements of proton intensities in ICME, we can also find that the local acceleration efficiency is energy-dependent, decreasing from lower to higher energies.

Using the selection method described before, we find 12 energetic-particle-enhanced ICMEs. In other words, only $\sim 2\%$ of ICMEs contain enhanced energetic particles. Of these 12 ICMEs, 9 have shocks inside, accounting for 75%. Moreover, if we raise the criteria and look for ICMEs in which the proton intensities increase in both of the two highest-energy channels (~ 4.5 and ~ 7 MeV), then we can only find seven energetic proton-enhanced ICMEs. All of them have shocks inside, demonstrating that shock-ICME interactions have a stronger ability to accelerate particles in ICMEs than other mechanisms. However, based on our ICME list together with the interplanetary shocks from the Center for Astrophysics (https://www.cfa.harvard.edu/shocks/wi_data) and the Finland heliospheric shock database (ipshocks.fi/database), we find that there are a total of 58 S-ICMEs observed by *Wind* during the period from 1995 to 2017. That is to say, although shock-ICMEs have higher probabilities of having enhanced energetic particles, only $\sim 16\%$ (9/58) of them are energetic-particle-enhanced.

3. Database

Table 1 lists the basic information of these 12 events, including the ICME beginning and end times and the energetic-particle enhancements compared to the upstream in every energy channel. Meanwhile, we also indicate whether the ICME is a S-ICME or an isolated ICME (I-ICME). During the period from 1995 to 2017, a total of 58 S-ICMEs and 429

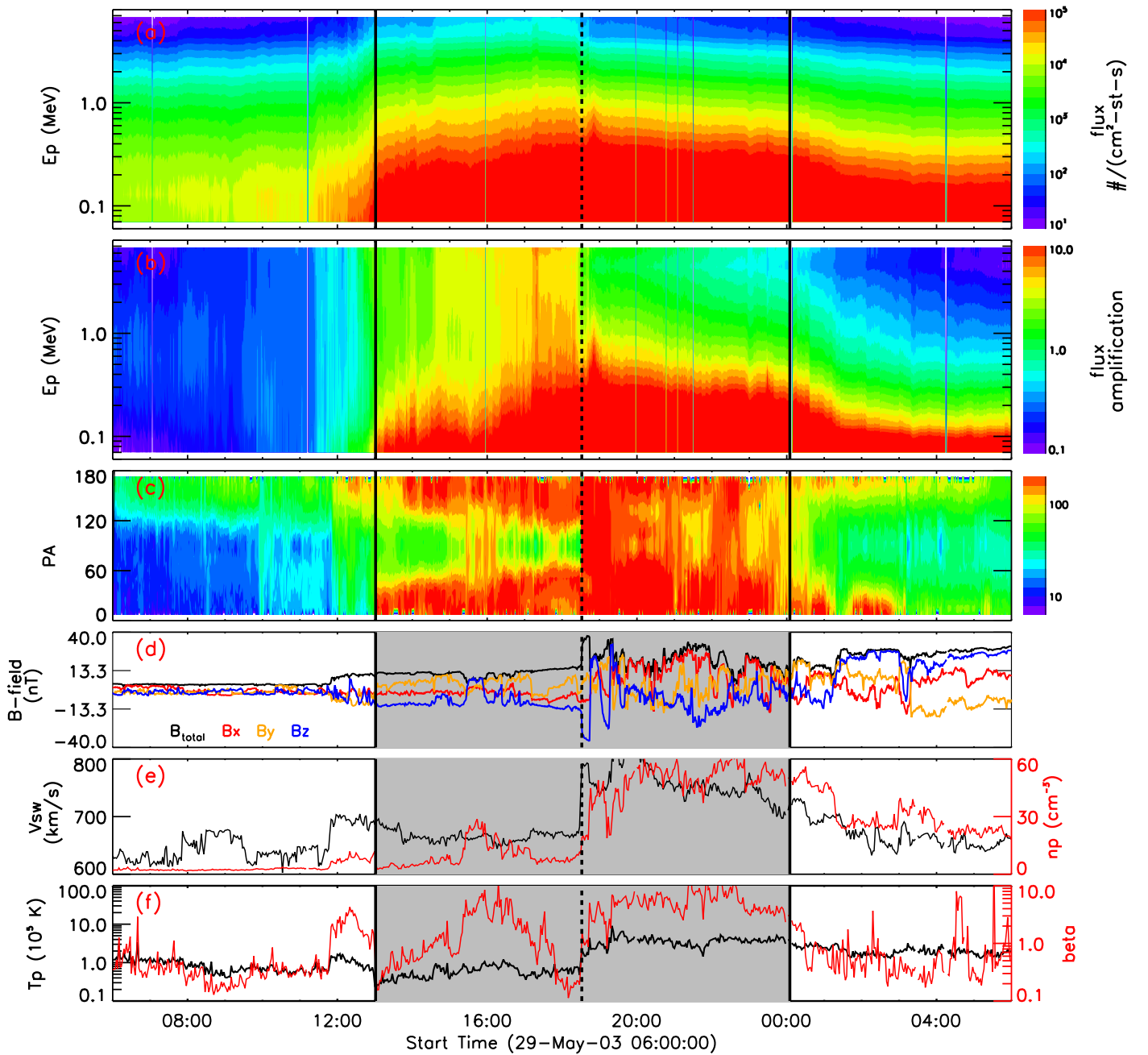


Figure 1. Wind observations of an ICME on 2003 May 29. From top to the bottom, panels are the distribution of energetic proton intensities in seven energy channels, the normalized energetic proton intensities, the suprathermal electron pitch-angle distribution, magnetic-field strength, (B) and three components of magnetic-field vector in GSE coordinate, solar-wind speed (v), and proton density (N_p), proton temperature (T_p), and β . The shaded region shows the period of the ICME, and the vertical dashed black line inside represents the shock.

I-ICMEs were observed by *Wind* spacecraft. 9 out of the 58 S-ICMEs and 3 of the 429 I-ICMEs had enhanced energetic particles. A comparison of these two kinds of ICMEs with energetic-particle enhancements will be presented in Section 4. Note that the energetic-particle-enhanced ICME on 2001 November 5 reported by Shen2008 is not included in our database, as the energetic-particle intensities in the downstream are no lower than those inside the ICME except for the two highest-energy channels. In this table, we can roughly see that the occurrence of these ICMEs with energetic-particle enhancements tracks the overall occurrence of the ICMEs with shocks, as found by Chi et al. (2016). More cases occur in the solar maximum than in the solar minimum.

4. Comparison between Two Kinds of ICMEs with Enhanced Energetic Particle Intensities

As we have mentioned before, 3 of 429 I-ICMEs and 9 out of 58 S-ICMEs have energetic-particle enhancements, showing that S-ICMEs are more likely to have enhanced energetic-particle intensities. Just as mentioned in Shen2008, the energetic-particle enhancements in S-ICMEs might be due to the combined effects of the shock and the MC boundaries. As for the other 3 I-ICMEs, the accelerators in them are unclear. On one hand, these enhanced energetic particles could be caused by the interactions between the ICMEs and other structures, such as the trailing stream interaction regions

Table 1
Information of the 12 ICMEs with Enhanced Energetic Particle Intensities

| ICME Begin | ICME End | Type | Enhancements | | | | | | |
|---------------------|---------------------|--------|--------------|---------|---------|-------|-------|---------|-------|
| | | | 200 keV | 330 keV | 550 keV | 1 MeV | 2 MeV | 4.5 MeV | 7 MeV |
| 2000-09-02T23:28:30 | 2000-09-03T13:48:00 | I-ICME | 2.00 | 2.19 | 2.67 | 2.96 | 2.58 | 1.67 | 1.15 |
| 2013-06-06T14:45:50 | 2013-06-07T12:12:50 | I-ICME | 3.63 | 3.05 | 2.83 | 2.54 | 2.23 | 1.31 | 1.09 |
| 2015-07-13T01:17:08 | 2015-07-14T21:42:51 | I-ICME | 43.13 | 42.07 | 35.80 | 30.21 | 17.15 | 4.33 | 1.53 |
| 1999-02-17T12:22:30 | 1999-02-18T10:30:00 | S-ICME | 17.99 | 26.80 | 27.45 | 19.87 | 10.98 | 7.58 | 6.92 |
| 2000-02-11T16:17:37 | 2000-02-12T02:55:07 | S-ICME | 1.57 | 2.03 | 3.11 | 4.26 | 6.11 | 6.08 | 4.86 |
| 2000-08-10T20:20:37 | 2000-08-12T01:13:07 | S-ICME | 3.97 | 3.32 | 3.02 | 2.66 | 2.33 | 2.21 | 2.37 |
| 2000-10-03T12:09:00 | 2000-10-05T06:27:00 | S-ICME | 14.41 | 8.90 | 5.54 | 4.09 | 2.48 | 1.66 | 1.62 |
| 2001-10-27T02:19:30 | 2001-10-28T05:21:22 | S-ICME | 1.89 | 3.01 | 4.32 | 5.36 | 5.74 | 5.14 | 7.50 |
| 2003-05-29T13:00:45 | 2003-05-30T00:04:30 | S-ICME | 12.42 | 7.65 | 5.19 | 4.42 | 3.56 | 3.45 | 3.39 |
| 2010-02-15T11:53:48 | 2010-02-15T22:28:18 | S-ICME | 7.01 | 6.53 | 5.32 | 4.08 | 2.57 | 1.99 | 1.22 |
| 2014-02-19T11:43:55 | 2014-02-20T05:51:00 | S-ICME | 52.46 | 53.47 | 47.99 | 38.80 | 28.04 | 17.20 | 21.59 |
| 2017-09-07T16:50:00 | 2017-09-08T01:00:00 | S-ICME | 3.32 | 4.64 | 6.55 | 7.57 | 5.04 | 3.16 | 3.13 |

(SIRs; e.g., Crooker et al. 1999; Mason & Sanderson 1999; Richardson 2004; Wei et al. 2019) or coronal mass ejections (CMEs; e.g., Gosling et al. 2005; Lugaz et al. 2008; Farrugia et al. 2011). Or even that these events are caused by the shock-ICME interactions, but the shocks have been dissipated during the propagation inside the ICMEs due to the relatively large Alfvénic speed (e.g., Lugaz et al. 2015). On the other hand, in situ evidence that electrons and ions are energized in solar-wind regions filled with magnetic islands or plasmoids has emerged in the past few years (e.g., Drake et al. 2006; Zank et al. 2014). People believed that reconnection-associated merging and contracting plasmoids can lead to the first-order Fermi energization of electrons and ions of initially moderate energies trapped in the islands (e.g., Zank et al. 2015; Zhao et al. 2018, 2019). However, are their acceleration efficiencies comparable to the shock-ICME interaction? To answer this question, we compare the performances of the enhanced energetic particles in the two kinds of ICMEs.

Table 1 shows us the increase of energetic-particle intensities in different energy channels for the nine S-ICMEs and three I-ICMEs. By some simple calculations, we can find that the median intensity enhancements of the nine S-ICMEs in the seven energy channels are 7.0, 6.5, 5.3, 4.4, 5.0, 3.4, and 3.4. And the values of the three I-ICMEs are 3.6, 3.1, 2.8, 3.0, 2.6, 1.7, and 1.2, respectively. This indicates that particle intensities increase most obviously at the lower-energy channels. Additionally, in all energy channels, the flux enhancements are more pronounced in S-ICMEs than in I-ICMEs.

Energetic spectra, showing the accumulated particle intensity at a given time period versus the particle energy, provide another powerful way to judge the intensities of SEP events. In order to fit the spectra more accurately, we need to use more data points. Here, apart from the energetic-particle measurements obtained by *Wind*/3dp, we also adopt the data from the Electron, Proton, and Alpha Monitor (EPAM) particle instrument on *ACE* (Gold et al. 1998). It measures the fluxes and directions of ions greater than 50 keV. Because the locations of the *Wind* and *ACE* satellites are not exactly the same, we do the time shift calibration for the *ACE* data. For the S-ICMEs, the time shift calibration is based on the arrival times of the shocks inside ICMEs at the two satellites. For the I-ICME event, the calibration is based on the distance between the two satellites and the speed of the ICME.

Using 7 energy channels from *Wind*/3dp together with 6 energy channels from *ACE*/EPAM, we fit the energy spectra of

all 12 ICME events with the energy from 0.1 MeV to about 4 MeV. Since the durations of the ICME and the defined ICME upstream (1–4 hr before the ICME begin time) are different, for the sake of comparison, we fit the averaged energetic proton intensities in the upstream and ICME intervals for each event. In addition, unlike most papers that calculate the spectra of energetic particles, we focus on a comparison of the spectra indices in the ICME internal and upstream, therefore the pre-ICME energetic-particle intensities are not subtracted from those measured inside the ICME when fitting the ICMEs. The spectra are fitted by a power-law function:

$$\frac{dJ}{dE} = KE^{-\gamma}. \quad (1)$$

Here, J is the particle intensity, K and γ are constants, and E is measured in energy/nucleon.

Figure 2 shows the spectra for the energetic particles in the upstream and ICME intervals of the 12 events. Each panel shows an event, with panels (a) through (i) representing the nine S-ICME events and panels (j) through (l) representing the three I-ICME events. Spectra taken from the upstream and the ICME interval are shown in black and red in each panel, respectively. The fitted K and γ values are also marked in the lower left corner of each panel.

Seen from this figure, the values of K are enhanced in the ICME intervals for all events. On average, the K values fitted in the ICME intervals increase by seven times compared with those fitted in the upstream. This phenomenon makes sense, as these events are all selected events that have enhanced particle intensities. In addition, in S-ICMEs, the enhancements of K range from 3.4 to 13.1, with a median value of 5.5, while in the I-ICMEs, the enhancements of K are 3.5, 2.7, and 18.2, with a median value of 3.5. That is to say, K values increase more in S-ICMEs than in I-ICMEs, indicating that the proton intensity enhancements are more pronounced in S-ICMEs than in I-ICMEs. This is consistent with Table 1, which shows that the energetic-particle intensities increase more in the S-ICMEs than in the I-ICMEs in all energy channels.

Furthermore, for most events, the values of γ in the ICMEs are greater than those before the ICMEs, with only three exceptions. The three events happened on 2000 February 11, August 11, and 2001 October 27. All of them are S-ICME events. On average, the values of γ increase by a factor of ~ 1.08 in S-ICMEs, while in I-ICMEs, they increase by ~ 1.10 times. Since the larger the γ value, the faster the particle

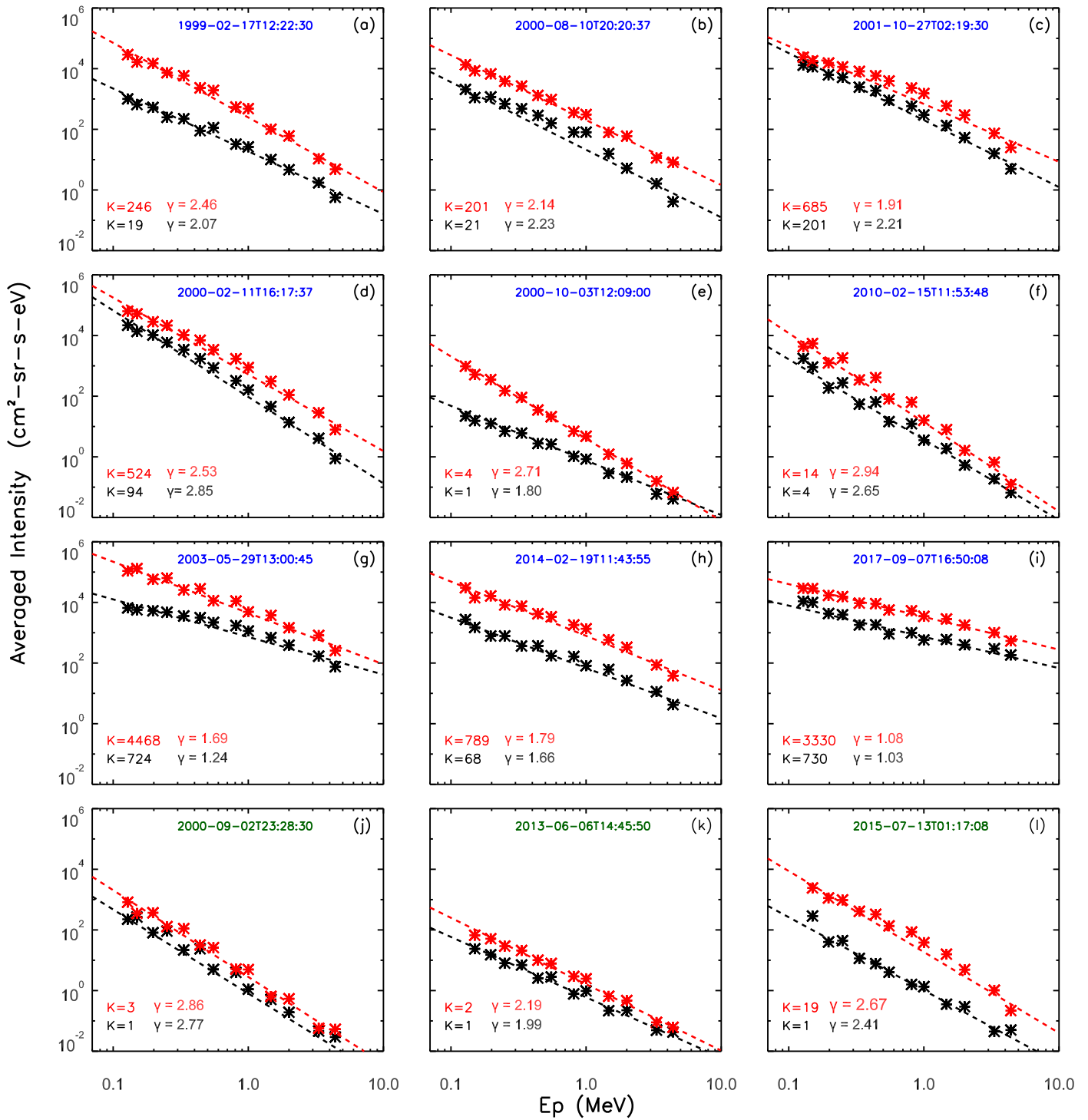


Figure 2. Averaged proton spectra taken from the upstream (black) and the ICME intervals (red) in the 12 energetic-particle-enhanced ICME events. Panels (a)–(i) represent the nine S-ICMEs and panels (j)–(l) represent the three I-ICMEs. The ICME begin times in each event are indicated in the upper right corner.

intensities decrease with the increase of energy, the increase of γ values in ICME intervals demonstrates that the proton enhancements are energy-dependent, decreasing from lower energies to higher energies. Energetic protons with low energies are most obviously enhanced. Additionally, the more obvious increase of γ in I-ICMEs indicates that the increase of protons with high energy in them is more limited. Overall, through comparing the increase of K and γ in S-ICMEs and I-ICMEs, it can be found that in all energy channels, especially

high-energy channels, the proton intensity enhancements are more pronounced in S-ICMEs than in I-ICMEs.

5. Uniqueness of the S-ICMEs with Enhanced Energetic Particle Intensities

According to our survey, not all S-ICME structures are accompanied by enhanced energetic-particle intensities. Only about 16% (9/58) of S-ICMEs have enhanced energetic-particle

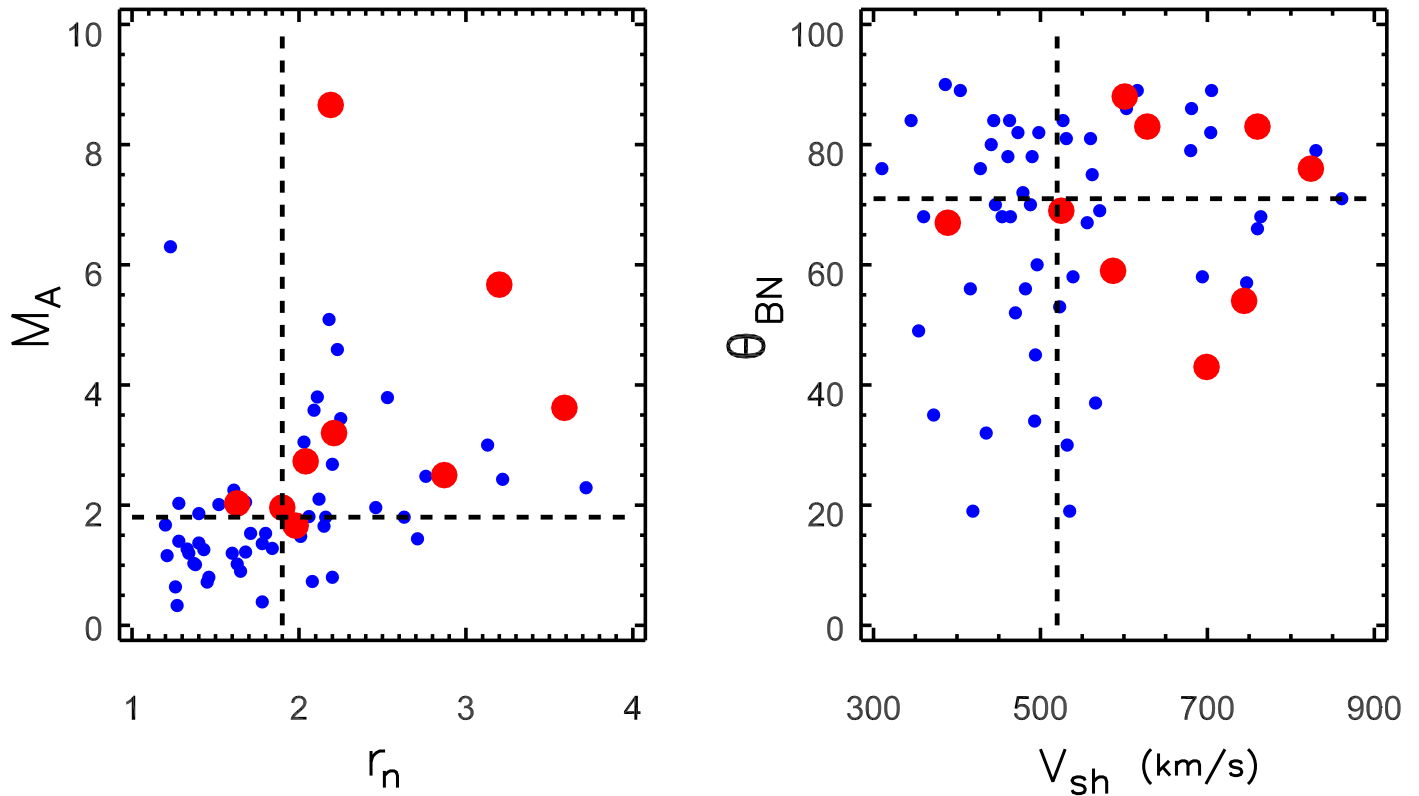


Figure 3. Scatter plot of the parameters of shocks inside ICMEs. The blue dots represent all 58 shocks inside ICMEs observed by *Wind* from 1995 to 2017. The bold red dots represent those nine shocks that lead to enhanced energetic-particle intensities through interaction with the host ICMEs. The dashed lines in the two panels mark the median values of the 58 shocks.

Table 2
Parameters of the Nine Shocks Inside ICMEs

| Shock Time | \hat{n} | V_{sh} (km s $^{-1}$) | r_n | M_A | θ_{BN} |
|---------------------|-----------------------|---------------------------------|-------|-------|----------------------|
| 1999-02-18T02:48:15 | [−0.98, −0.18, −0.02] | 699 | 3.2 | 5.67 | 43 |
| 2000-02-11T23:33:54 | [−0.81, −0.38, 0.44] | 601 | 3.59 | 3.62 | 88 |
| 2000-08-11T18:49:36 | [−0.98, −0.11, −0.13] | 628 | 1.98 | 1.66 | 83 |
| 2000-10-05T03:28:42 | [−0.92, −0.13, 0.38] | 525 | 2.21 | 3.2 | 69 |
| 2001-10-28T03:13:48 | [−0.96, 0.28, 0.06] | 587 | 2.87 | 2.5 | 59 |
| 2003-05-29T18:31:09 | [−0.91, 0.42, 0.08] | 824 | 1.89 | 1.96 | 76 |
| 2010-02-15T17:39:24 | [−0.95, −0.26, 0.16] | 389 | 1.63 | 2.03 | 67 |
| 2014-02-20T02:42:00 | [−0.89, −0.24, 0.39] | 760 | 2.19 | 8.66 | 83 |
| 2017-09-07T22:28:00 | [−0.83, 0.3, −0.46] | 759 | 2.23 | 2.73 | 54 |

intensities. So, how are these events different from other S-ICME structures? As we all know, the shock intensity plays an important role in the particle acceleration. Therefore, we want to analyze the uniqueness of the nine S-ICMEs in terms of shock properties. Table 2 displays the characteristics of these nine shocks, including the shock time, shock normal (\hat{n}) in GSE coordinates, speed (V_{sh}), density compression ratio (r_n), Alfvén mach number (M_A), and the angle between the shock normal and the upstream magnetic-field vector (θ_{BN}). The shock parameters are obtained by nonlinear least-squares fitting of the incomplete Rankine–Hugoniot relations (temperature information is not used) originally developed by Viñas & Scudder (1985) and further enhanced by Szabo (1994).

Figure 3 is the scatter plot of the parameters of shocks inside ICMEs. The blue dots represent all 58 shocks inside ICMEs observed by *Wind* from 1995 to 2017. The bold red dots in the

figure mark those nine shocks that lead to enhanced energetic-particle intensities through interaction with the host ICMEs. In the left panel, the horizontal axis shows the shock density compression ratio (r_n) and the vertical axis shows the shock Alfvén mach number (M_A). In the right panel, the horizontal axis is the shock speed (V_{sh}) and the vertical axis is (θ_{BN}). In each panel, the dashed lines represent the median values of all 58 shocks inside ICMEs. As we can see from the figure, most of these nine shocks have relatively high speeds as well as relatively large density compression ratios and Alfvén mach numbers. Because these three parameters are widely used to indicate the shock strength, we think that the acceleration of the energetic particles in the S-ICMEs is related to the shock. Additionally, there is nothing unusual about the θ_{BN} of these 9 shocks. Both of them show a clear bias toward quasi-perpendicular shock. The median values of θ_{BN} for these two

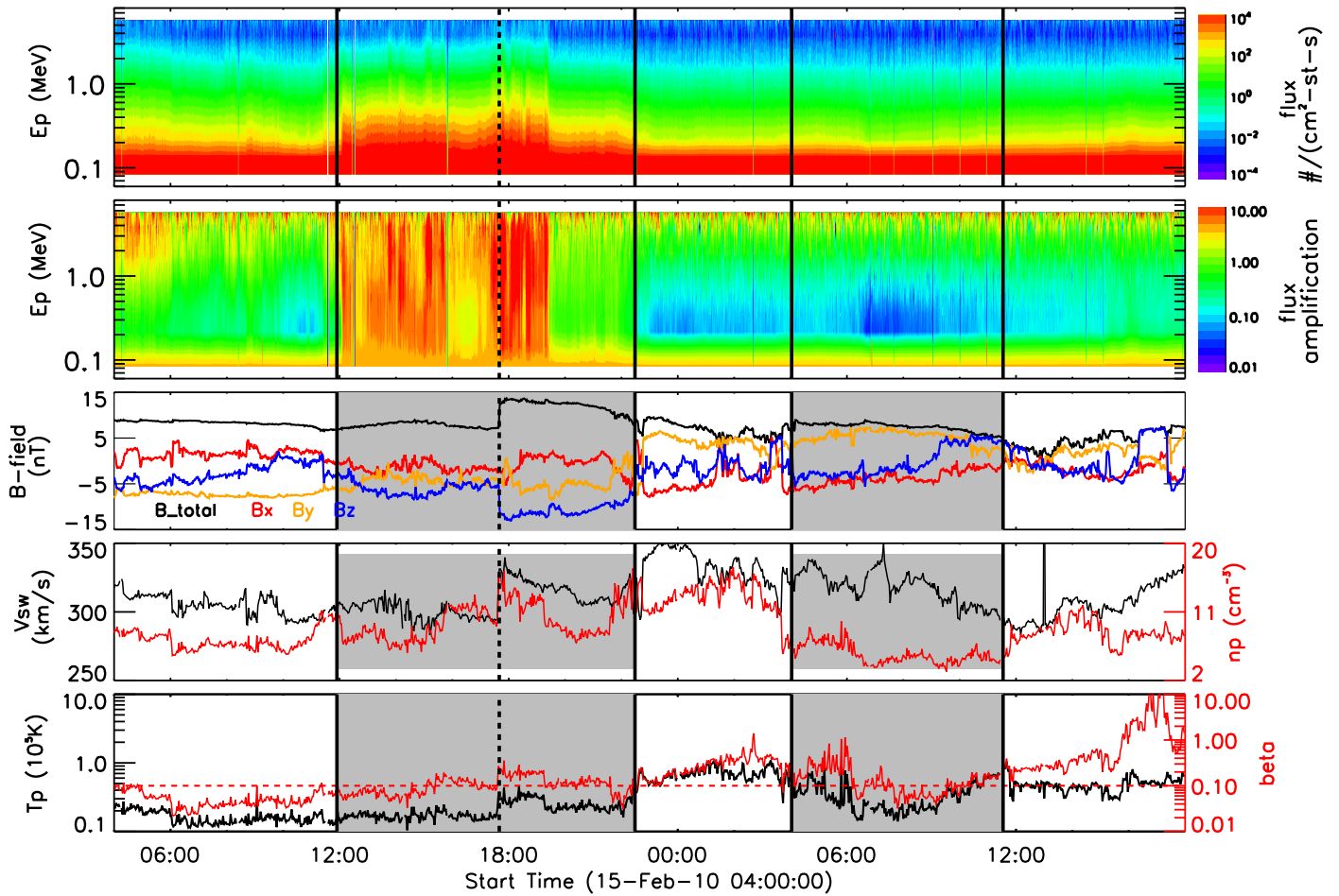


Figure 4. Wind observations from 2010 February 15 04:00 UT to 2010 February 16 18:00 UT. From top to the bottom, the panels show the distribution of energetic proton intensities in seven energy channels, the normalized energetic proton intensities, magnetic-field strength (B), and three components of magnetic-field vector in GSE coordinate, solar-wind speed (v), and proton density (N_p), proton temperature (T_p), and β . The shaded regions show the periods of the ICMEs and the vertical dashed line represents a fast forward shock.

kinds of shocks are 71° and 69° . This is consistent with previous statistical results, that is, most of the shocks observed near the earth are quasi-perpendicular shocks (Kilpua et al. 2015).

The study of energetic-particle-enhanced S-ICME in our work is similar to previous studies of energetic storm particle (ESP) events, which are characterized by the energetic-particle enhancements associated with the shock local acceleration. The difference is that in our cases, the ESP should occur in ICMEs. Using the *ACE*/EPAM data as a measure, Lario et al. (2003) studied the intensity changes of 47–4800 keV ions at 168 shocks, finding that only 33% shocks lead to enhancements of 1.9–4.8 MeV ions. In addition, the energetic-particle intensities were usually found to peak within ~ 2 minutes of the shock passage, with a clear trend toward occurrence in the downstream region of the shock. Kallenrode (1996) studied the enhancements of 5 MeV protons associated with 351 shocks observed by *Helios* between 1974 and 1985, finding that the particle intensity at the shock, which could be used as a crude measure of the local shock acceleration efficiency, was correlated with the shock speed and magnetic compression ratio. This is consistent with our result that faster and stronger shocks have higher probabilities of accelerating particles locally. However, through searching the responses of >10 MeV energetic particles to 354 shocks observed by

ACE, Cohen et al. (2005) claimed that the size of the ESP event (i.e., intensity increase factor) did not appear to be dependent on either the shock speed or the θ_{BN} values.

However, according to the shock information given in Table 2, we also have to admit that not all strong shocks lead to enhanced energetic particles intensities in the S-ICMEs, as shown in Figure 3. This may indicate that the strength of the shock cannot fully represent its particle acceleration efficiency. As previous studies have shown, the abundance of the seed particles plays an important role in particle acceleration (e.g., Gopalswamy et al. 2004; Mewaldt et al. 2006, 2012; Li et al. 2012; Reames 2015). So maybe there are not enough seed particles in those events. Moreover, not all nine S-ICMEs structures possess fast and strong shocks. For example, the shock on 2010 February 15 has a velocity of only about 389 km s^{-1} and a density compression ratio of 1.63. However, it leads to energetic-particle enhancements in five energy channels.

Figure 4 shows the in situ observations of this S-ICME. The shock driven by the subsequent ICME (the second shaded region) propagates into the leading ICME (the first shaded region) and forms an S-ICME. It is worth noting that these two ICMEs are not included in the ICME list established by Richardson and Cane (<http://www.srl.caltech.edu/ACE/ASC/DATA/level3/icmetable2.htm>, Richardson & Cane 2010). The

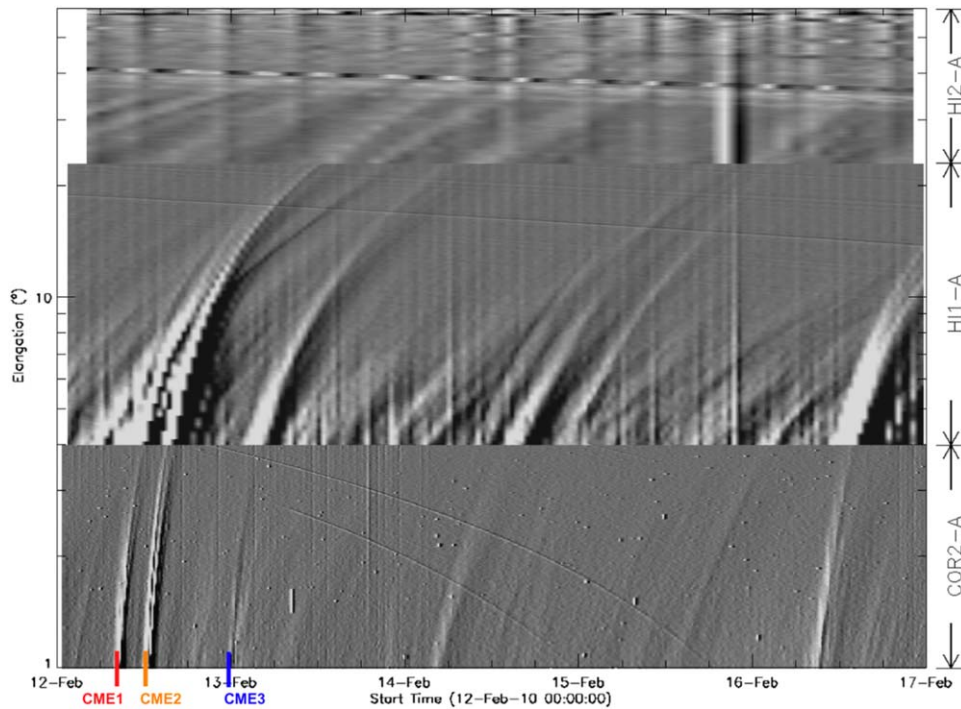


Figure 5. Time-elongation angle map based on *STEREO-A* observations from 2010 February 12 to 17. Three CMEs starting at 08:39 UT, 12:39 UT, and 23:45 UT on February 12 are marked on the map.

first two panels show that the energetic-particle intensities increase significantly during the entire period of the shock-ICME structure. Why can such a slow and weak shock accelerate particles in the ICME? Our conjecture is that this shock used to be fast when it entered the ICME and the energetic particles are accelerated at that time. The accelerated particles were confined in the ICME interval and arrived at Earth with the ICME. The shock was dissipated during the propagation inside the ICME due to the relatively large Alfvénic speed, so when it arrived, we only saw a very slow shock.

To test our idea, we refer to the coronagraph observations. We find that three CMEs occurred on February 12. Figure 5 shows the J-map from 2010 February 12 to 17. A 64 pixel-wide slice is placed eastward along the ecliptic plane in the running-difference images from COR2, HI1, and HI2 on board *STEREO-A* to produce this J-map. Three tracks starting at 08:39 UT, 12:39 UT, and 23:45 UT on February 12 can be seen in the map, corresponding to the propagation of the three CMEs (CME1, CME2, and CME3, respectively). However, based on the observation near the Earth, we only find two ICMEs. Which CME is the source of the second ICME on February 16: the CME at 12:39 UT (CME2) or the CME at 23:45 UT (CME3)? In order to answer this question, we adopt the geometric triangulation technique (Liu et al. 2010; Ying et al. 2010), applied to COR2, HI1, and HI2 on *STEREO-A* and B, to analyze the kinematics of these two CMEs. The results show that CME2 basically propagates along the Sun–Earth line, and the estimated arrival time is 04:46 UT on February 16, which is very close to the beginning of the second ICME. While the propagation direction of CME3 is generally between W25 and W35 and the estimated time to reach 1 au is 04:40 UT on February 17, which is about 1 day after the start of the second ICME. In addition, we do the GCS fitting (e.g., Thernisien et al. 2006, 2009; Thernisien 2011) for CME3, finding that it is a very narrow CME with a half angular width

of 20° . Considering that its propagation direction is about 30° west to the Sun–Earth line, we think that it is hard for CME3 to arrive at Earth. According to the above analyses, we consider the second ICME to be the counterpart of CME2 instead of CME3.

After confirming CME2 as the source of the second ICME, we then focus on calculating the speed of the shock it drove. Figure 6 shows the coronagraph observations of CME2 from *STEREO-B/COR2*, *SOHO/LASCO*, and *STEREO-A/COR2*. It is clear that this CME drove a shock in front of it from the observations of *STEREO-B* and *SOHO*. The shock and the CME are further fitted with a spheroid and a GCS flux rope, and the results are overlaid on the coronagraph observations in the lower panels. Using the fitting results of the shock heights at five different times in the *STEREO-B* observations, we find that the shock speed is 714 km s^{-1} (Figure 7). This is not a slow speed for shocks near the Sun, so we confirm that it is the propagation inside the first CME that decelerates the shock.

6. Energetic Particle Acceleration in I-ICMEs

As we have mentioned before, there are three energetic-particle-enhanced I-ICMEs in which the particle acceleration mechanisms are unclear. Here we briefly discuss the possible accelerators in these three events.

Figure 8 displays the I-ICME event that happened on 2000 September 3. We can find that there is a period of enhanced energetic-particle intensities in the first half of the ICME. If we look closely at the magnetic field and solar-wind data inside the ICME, there are actually two interacting ICMEs in it. The interaction region is marked by two vertical green lines. It is characterized by a sudden decrease in the strength of the magnetic field together with increased proton density, temperature, and β (Wang et al. 2003). So in this case, CME–CME interaction may be the cause of enhanced energetic-particle

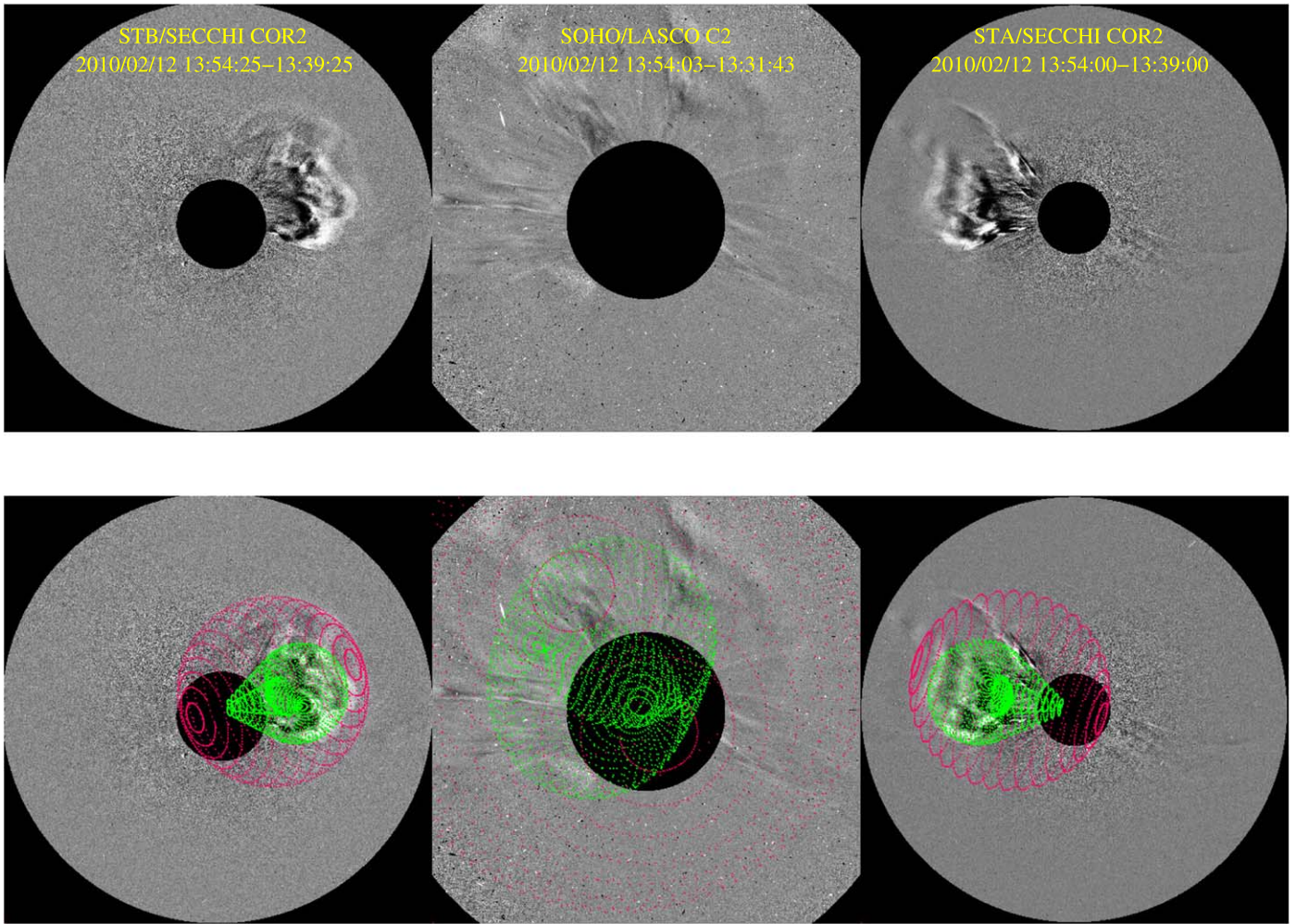


Figure 6. Top: running-difference coronagraph images of the second CME and shock from *STEREO-B* (left), *SOHO* (middle), and *STEREO-A* (right). Bottom: the coronagraph images of these CMEs with GCS wireframes overlaid on top. The green wireframe represents the CME and the red wireframe represents the shock.

intensities. The second CME may have driven a shock that entered the first CME and accelerated particles. However, by the time the first ICME reached the Earth, the inner shock had already been dissipated. So we did not see a shock-ICME structure.

The event on 2013 June 6 is similar. Figure 9 shows the observation. The proton intensity enhancements in this event extend over the entire period of the ICME, especially in the middle part. The observations of the solar wind and magnetic field show that this ICME also contains two interacting ICMEs. The interaction region is marked by two vertical green lines. For this event, thanks to the combined coronagraph observations from *STEREO* and *SOHO*, we find the corresponding source CMEs happened on 2013 June 2 successively. The three views on the two CMEs offered by *STEREO-A* and *-B* and *SOHO* are shown in Figure 10. In the bottom panels, the GCS fitting results of the first and second CMEs (green wireframe and red wireframe) are superposed on the coronagraph images. The propagation directions of these two CMEs are S57E0 and S05E06, respectively. Both of the CMEs are slow, with the second one being relatively faster. Their speeds are 300 km s^{-1} and 369 km s^{-1} , respectively. In this case, the interaction between the two CMEs may contribute to the enhanced energetic-particle intensities.

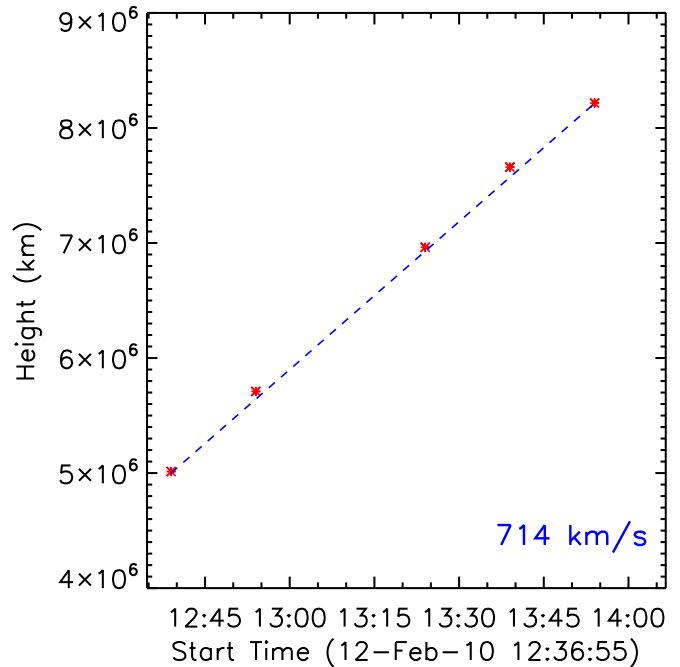


Figure 7. Height of the CME-driven shock from the GCS fitting results at five different times. The shock velocity obtained by the linear fitting method is 714 km s^{-1} .

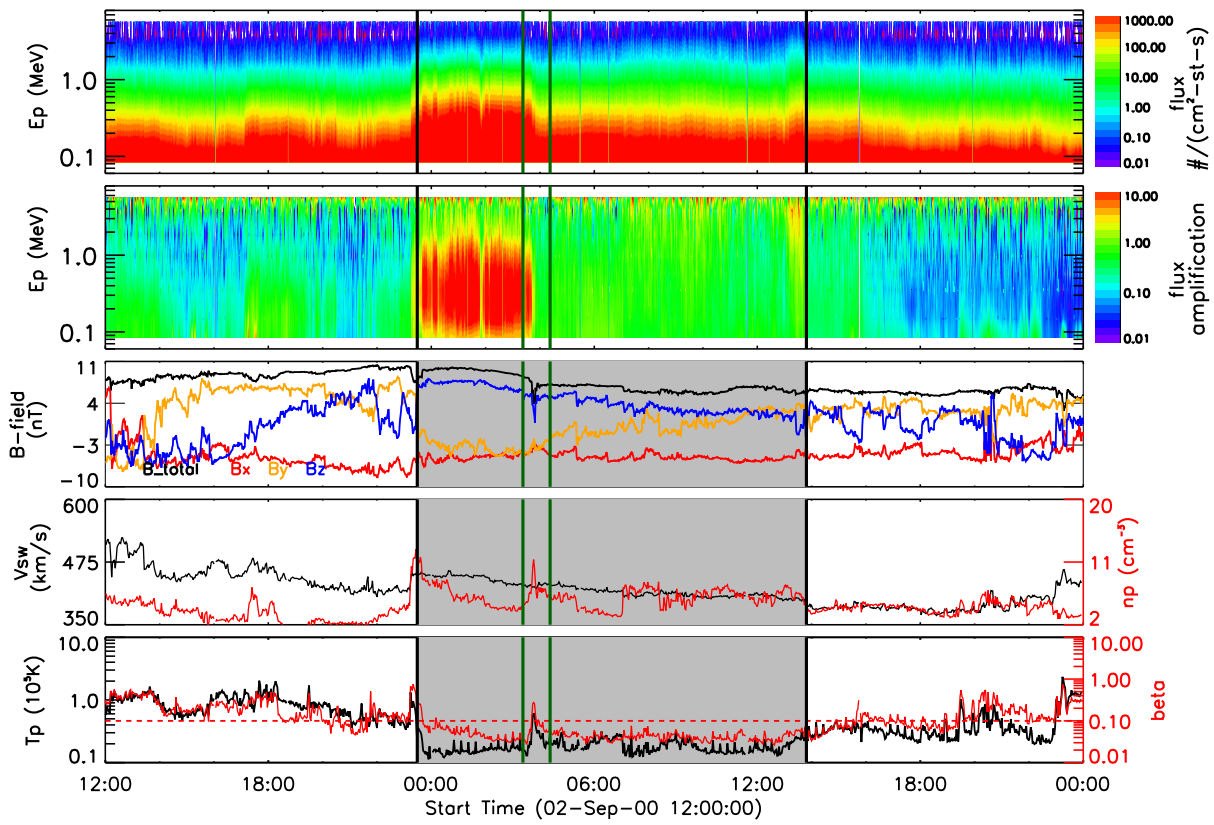


Figure 8. Wind observations of an energetic-particle-enhanced I-CME on 2000 September 2. This ICME actually consists of two interacting ICMEs. The interaction region is marked by the two vertical green lines.

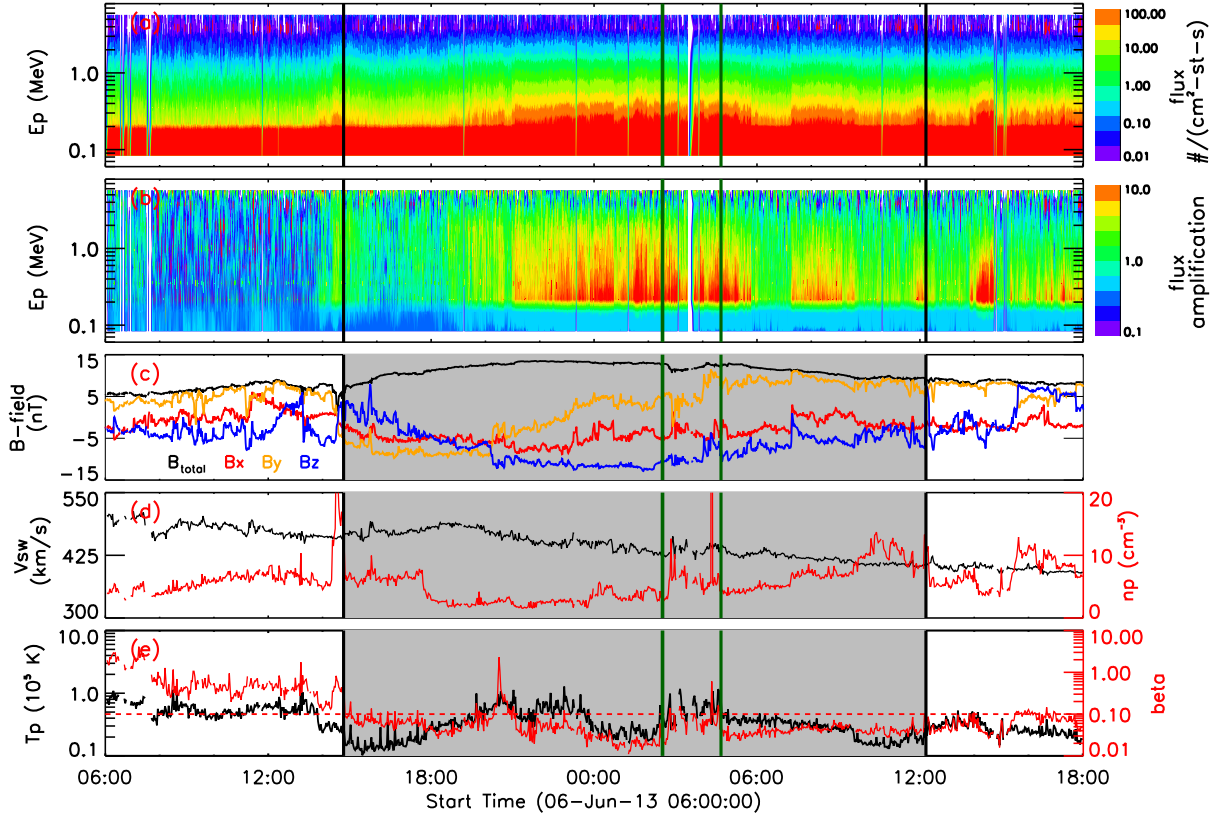


Figure 9. Wind observations of an energetic-particle-enhanced I-CME on 2013 June 6. This ICME also consists of two interacting ICMEs. The interaction region is marked by the two vertical green lines.

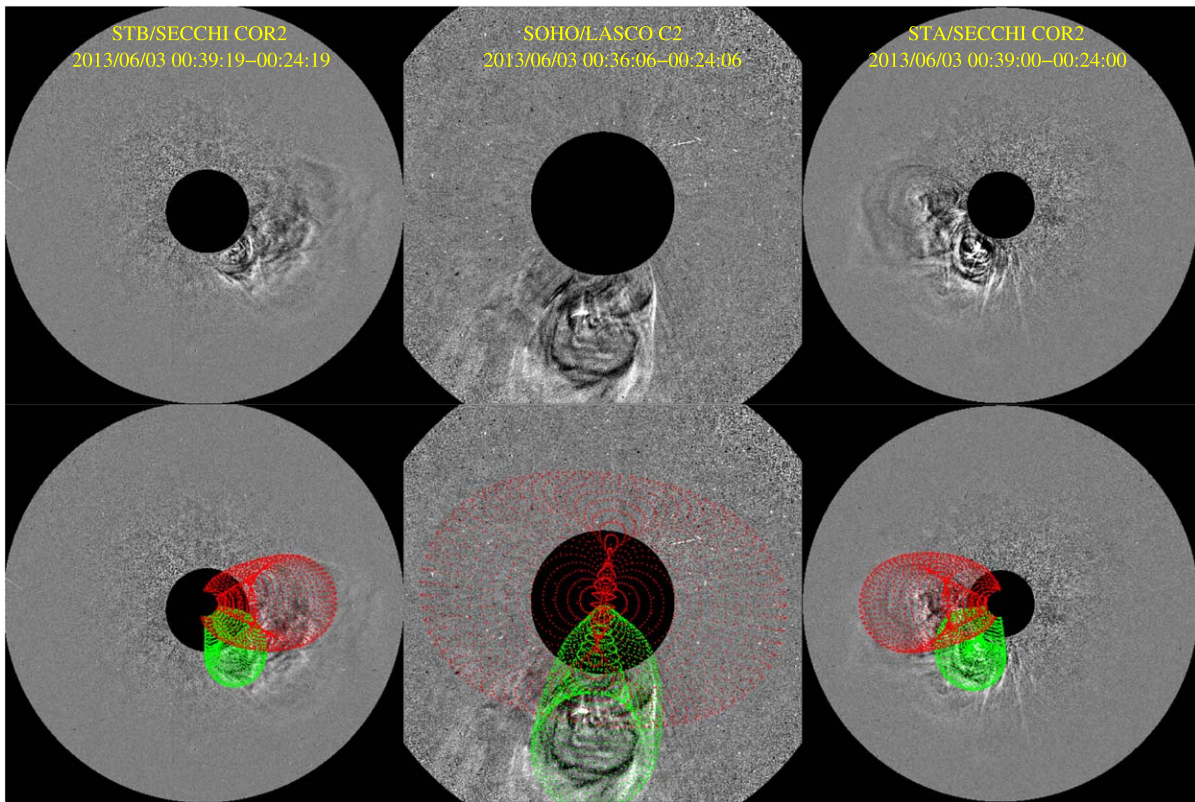


Figure 10. Top: running-difference coronagraph images of the two CMEs from *STEREO-B* (left), *SOHO* (middle), and *STEREO-A* (right). Bottom: coronagraph images of these CMEs with a GCS wireframe overlaid on top. The green wireframe represents the first CME and the red wireframe represents the second CME.

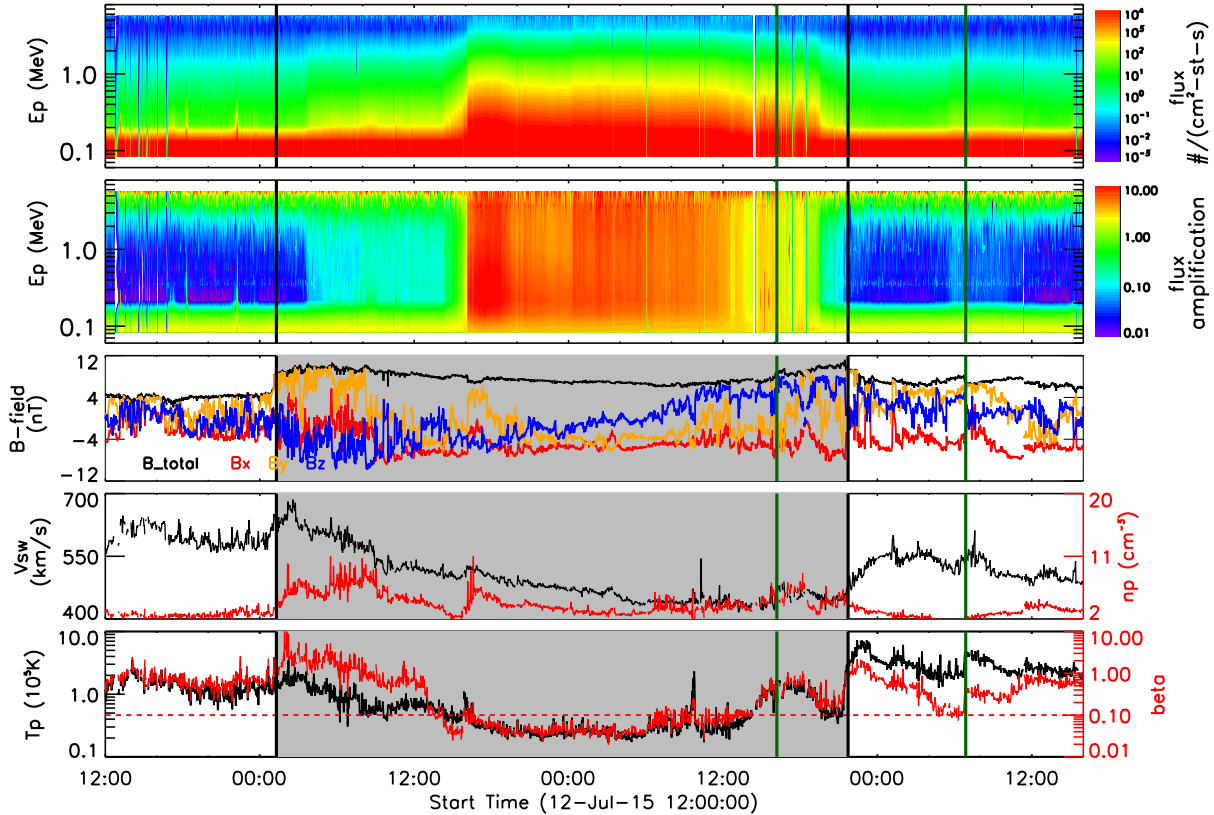


Figure 11. Wind observations of an energetic-particle-enhanced ICME on 2015 July 13. This ICME is followed by a SIR, which is between the two vertical green lines in the figure.

On the other hand, Figure 11 shows that the energetic-particle-enhanced I-ICME event happened on 2015 July 13. In this case, the intensities of the high-energy particles increase conspicuously. For 1 MeV protons, the particle intensity increases more than 30 times in the ICME interval. This figure shows that this ICME is followed by a SIR that has increasing solar-wind speed and increased temperature. In addition, its density increases and then decrease. The SIR interval is marked by the two vertical green lines in the figure. In this case the compression of the SIR on the ICME may lead to the particle acceleration (Giacalone et al. 2002; Kocharov et al. 2003).

Therefore, we consider that CME–CME interaction and CME–SIR interaction may contribute to the enhanced energetic-particle intensities in the three I-ICMEs.

7. Conclusion

In summary, using energetic-particle observations from *Wind*/3dp during the period from 1995 to 2017, we find that of 487 ICMEs, 12 have extraordinary energetic-particle enhancements. These cases are very different from the usual picture in which energetic particles are depressed in ICMEs. Of these 12 ICMEs, 9 have shocks inside, 75%. Through analyzing these events, we find that:

1. The occurrence rates of these 12 ICMEs follow the change of sunspot number, indicating that the particle acceleration mechanisms in these events may be related to the intensity of the solar activity.
2. Of 58 S-ICMEs, 9 have enhanced energetic-particle intensities. In addition, energetic particles increase more in the S-ICMEs than in the I-ICMEs in all energy channels, especially in the high-energy channels.
3. Compared to other shocks in ICMEs, the shocks in energetic-particle-enhanced ICMEs have relatively higher speeds, density compression ratios, and Alfvén mach numbers. This may indicate that the acceleration of the energetic particles in the S-ICMEs is related to the shock.

This work is supported by grants from CAS (Key Research Program of Frontier Sciences QYZDB-SSW-DQC015), NSFC (41822405, 41774181, 41774178, 41574165, 41474164, 41761134088, 41904151), the Fundamental Research Funds for the Central Universities (WK2080000077), the Specialized Research Fund for State Key Laboratories, and the key research program of the CAS (XDPB11), Anhui Provincial Natural Science Foundation (1908085MD107), Project funded by China Postdoctoral Science Foundation (2019M652194).

ORCID iDs

Yuming Wang  <https://orcid.org/0000-0002-8887-3919>
 Qiang Hu  <https://orcid.org/0000-0002-7570-2301>
 Gang Li  <https://orcid.org/0000-0003-4695-8866>

References

- Burlaga, L., Sittler, E., Mariani, F., & Schwenn, R. 1981, *JGRA*, **86**, 6673
 Cane, H., & Lario, D. 2006, *SSRv*, **123**, 45
 Chi, Y., Shen, C., Wang, Y., et al. 2016, *SoPh*, **291**, 2419
 Cohen, C. M. S., Mewaldt, R. A., Smith, C. W., et al. 2005, ICRC (Pune), **29**, 327
 Crooker, N. U., Gosling, J. T., Bothmer, V., et al. 1999, *SSRv*, **89**, 179
 Drake, J. F., Swisdak, M., Che, H., & Shay, M. A. 2006, *Natur*, **443**, 553
 Farrugia, C., Berdichevsky, D., Möstl, C., et al. 2011, *JASTP*, **73**, 1254
 Giacalone, J., Jokipii, J. R., & Kóta, J. 2002, *ApJ*, **573**, 845
 Gold, R., Krimigis, S., Hawkins, S., et al. 1998, *SSRv*, **86**, 541
 Gopalswamy, N., Yashiro, S., Krucker, S., Stenborg, G., & Howard, R. A. 2004, *JGRA*, **109**, A12105
 Gosling, J. T., Skoug, R. M., Mccomas, D. J., & Smith, C. W. 2005, *JGRA*, **110**, 1107
 Kahler, S. W., Krucker, S., & Szabo, A. 2011, *JGRA*, **116**, A01104
 Kallenrode, M. B. 1996, *JGR*, **101**, 24393
 Kallenrode, M.-B. 2001, *ICRC (Hamburg)*, **27**, 3273
 Kilpua, E., Lumme, E., Andreeva, K., Isavnin, A., & Koskinen, H. 2015, *JGRA*, **120**, 4112
 Kocharov, L., Kovaltsov, G. A., Torsti, J., Anttila, A., & Sahla, T. 2003, *JGRA*, **108**, 1404
 Lario, D. 2006, *Geophysical Monograph*, **165**, 309
 Lario, D., Decker, R. B., Livi, S., et al. 2005, *JGRA*, **110**, A09S11
 Lario, D., Ho, G. C., Decker, R. B., et al. 2003, in AIP Conf. Ser. 679, Solar Wind Ten, ed. M. Velli (Melville, NY: AIP), 640
 Li, G., Moore, R., Mewaldt, R. A., Zhao, L., & Labrador, A. W. 2012, *SSRv*, **171**, 141
 Lin, R. P., Anderson, K. A., Ashford, S., et al. 1995, *SSRv*, **71**, 125
 Liu, Y., Davies, J. A., Luhmann, J. G., et al. 2010, *ApJL*, **710**, L82
 Lugaz, N., Farrugia, C. J., Smith, C. W., & Paulson, K. 2015, *JGRA*, **120**, 2409
 Lugaz, N., Manchester, W. B., Roussev, I. I., & Gombosi, T. I. 2008, *JASTP*, **70**, 598
 Malandraki, O. E., Lario, D., Lanzerotti, L. J., et al. 2005, *JGRA*, **110**, A09S06
 Malandraki, O. E., Sarris, E. T., Lanzerotti, L. J., et al. 2002, *JASTP*, **64**, 517
 Mason, G., & Sanderson, T. 1999, *SSRv*, **89**, 77
 Mewaldt, R. A., Cohen, C. M. S., & Mason, G. M. 2006, *GMS*, **165**, 115
 Mewaldt, R. A., Mason, G. M., & Cohen, C. M. S. 2012, in AIP Conf. Ser. 1500, Space Weather: The Space Radiation Environment (New York: AIP), 128
 Reames, D. V. 2015, *SSRv*, **194**, 303
 Richardson, I. G. 1997, *GMS*, **99**, 189
 Richardson, I., & Cane, H. 2010, *SoPh*, **264**, 189
 Richardson, I. G. 2004, *SSRv*, **111**, 267
 Saiz, A., Ruffolo, D., Bieber, J. W., Evenson, P. A., & Pyle, R. 2008, *ApJ*, **672**, 650
 Shen, C., Wang, Y., Ye, P., & Wang, S. 2008, *SoPh*, **252**, 409
 Shen, C., Xu, M., Wang, Y., Chi, Y., & Luo, B. 2018, *ApJ*, **861**, 28
 Szabo, A. 1994, *JGRA*, **99**, 14737
 Tan, L. C., Malandraki, O. E., Reames, D. V., et al. 2012, *ApJ*, **750**, 146
 Thernisien, A. 2011, *ApJS*, **194**, 33
 Thernisien, A., Vourlidis, A., & Howard, R. A. 2009, *SoPh*, **256**, 111
 Thernisien, A. F. R., Howard, R. A., & Vourlidis, A. 2006, *ApJ*, **652**, 763
 Viñas, A. F., & Scudder, J. D. 1985, *JGR*, **91**, 39
 Wang, Y. M., Ye, P. Z., & Wang, S. 2003, *JGRA*, **108**, 1370
 Wei, W., Shen, F., Yang, Z., et al. 2019, *JASTP*, **182**, 155
 Ying, L., Thernisien, A., Luhmann, J. G., et al. 2010, *ApJ*, **722**, 1762
 Zank, G. P., Hunana, P., Mostafavi, P., et al. 2015, *JPhCS*, **642**, 012031
 Zank, G. P., le Roux, J. A., Webb, G. M., Dosch, A., & Khabarova, O. 2014, *ApJ*, **797**, 28
 Zhao, L., Zank, G., Chen, Y., et al. 2019, *ApJ*, **872**, 4
 Zhao, L., Zank, G., Khabarova, O., et al. 2018, *ApJL*, **864**, L34